Available online at www.sciencedirect.com
SCIENCE DIRECT®
International Journal of Machine Tools & Manufacture 46 (2006) 1369–1377
INTERNATIONAL JOURNAL OF MACHINE TOOLS & MANUFACTURE DESIGN, RESEARCH AND APPLICATION
www.elsevier.com/locate/ijmactool

Closed-form solutions for surface location error in milling

Tony L. Schmitz[a,*], Brian P. Mann[b]

[a]Department of Mechanical and Aerospace Engineering, University of Florida, Gainesville, FL, USA
[b]Department of Mechanical and Aerospace Engineering, University of Missouri, Columbia, MO, USA

Received 10 April 2005; accepted 10 October 2005
Available online 18 November 2005

Abstract

This paper provides two new analytical solutions for the computation of surface location errors, or part geometry errors that arise due to forced vibrations of the cutting tool, during stable milling. Prior studies of surface location error have applied numerical simulation and semi-analytical methods (e.g., temporal finite element analysis) to this problem. This work provides new results that show analytical solutions for the problem of surface location error are possible. The analytical approaches are based on frequency domain and harmonic balance analyses. Comparisons between the analytical results, time domain simulation, and experiment are included.
© 2005 Elsevier Ltd. All rights reserved.

Keywords: Milling; Forced vibration; Frequency response; Harmonic balance

1. Introduction

Process dynamics can impose severe limitations on milling efficiency. These limitations include: (1) chatter, or self-excited vibrations that lead to large forces, displacements, and poor surface quality; and (2) surface location error, or workpiece geometric inaccuracies that result from dynamic displacements of the tool and/or workpiece during stable (or time periodic) machining. Other limiting factors include, for example, machine tool quasi-static positioning errors, thermal errors, contouring errors, and tool wear.

Stability and surface location error in peripheral end milling may be determined using time domain simulation, where the tool displacements are obtained by numerical integration of the equations of motion, typically in two orthogonal directions within the plane of the cut (i.e., perpendicular to the tool axis) e.g., [1–13]. Generally, the cutting force is computed using the uncut chip area, which depends on both the current and time-delayed tool deflections, and appropriate cutting force coefficients. Models for the structural dynamics are typically based on modal parameters determined from a fit to a finite number of vibration modes. Although time domain simulation can conveniently incorporate such effects as the cutting edge helix angle, non-proportional teeth spacing, and runout, for example, searching large parameter domains in this manner is inefficient. Therefore, analytical solutions to the milling problem provide an attractive alternative. A primary goal of this work is to answer a current void in the literature through the introduction of two analytical solutions that give insight into the problem of surface location error with the inclusion of helix angle effects.

Milling is often described by a second-order differential equation that includes a time-delayed tool deflection term, which accounts for the interaction of the current tool motion with the surface left by the previous tooth passage. In stable cutting, the deflections are time periodic with tooth passage, so the time-delayed term is canceled by the current deflection [14]. Therefore, the stable milling solution can be treated as a linear non-homogeneous differential equation with constant coefficients. In the sections that follow, we solve the resulting forced vibration problem to determine surface location error using: (1) frequency domain; and (2) harmonic balance approaches.

2. Frequency domain solution

Early work by Arnold, Tlusty, Tobias, and Merrit identified *regeneration of waviness*, or the overcutting of the

*Corresponding author. Tel.: +352 392 8909; fax: +352 392 1071.
E-mail address: tschmitz@ufl.edu (T.L. Schmitz).

0890-6955/$ - see front matter © 2005 Elsevier Ltd. All rights reserved.
doi:10.1016/j.ijmachtools.2005.10.007

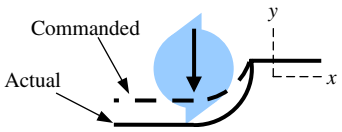

Fig. 1. Overcut surface in down milling due to the cutter position at the cut exit. The error is dominated by y-direction vibrations.

machined surface by the vibrating cutter, as a primary feedback mechanism for the growth of self-excited vibrations due to the modulation of the instantaneous chip thickness, cutting force variation, and subsequent tool vibration [15–21]. These studies led to the development of frequency domain solutions for process stability, where the information was presented in the form of stability lobe diagrams that identify stable and unstable cutting zones as a function of axial depth and spindle speed [22–25]. Clearly, a frequency domain surface location error solution would complement the frequency domain stability diagrams and provide a more complete picture of the role of milling dynamics on process efficiency.

A schematic of the surface location error phenomenon is provided in Fig. 1. Even under stable cutting conditions, the tool experiences periodic (forced) vibrations which depend on the system dynamic stiffness and excitation frequency, as well as other process parameters. The position of the tool in its periodic vibration cycle as it exits (down milling) or enters (up milling) the cut determines the actual location of the machined surface. Depending on the excitation frequency, which is governed by the spindle speed and number of teeth on the cutter, the surface may either be undercut (less material removed than commanded) or overcut (more material removed).

In order to determine surface location error using a frequency domain (or steady-state) approach, two basic assertions are made. First, although vibrations of the cutter occur in both the x- and y-directions (see Fig. 1), y-direction vibrations dominate the final surface location for an x-direction feed. Second, regeneration can be neglected in stable machining. Based on these assumptions, the concept is to: (1) express the y-direction cutting force in the frequency domain, $F_y(\omega)$ using a Fourier series; (2) determine the frequency domain y displacement, $Y(\omega)$, by multiplying $F_y(\omega)$ by the tool point frequency response function, or FRF, in the y-direction, $G_{yy}(\omega) = (Y(\omega)/F_y(\omega))F_y(\omega)$; and (3) inverse Fourier transform this result and sample at the cut entry (up milling) or exit (down milling) to find the surface location error.[1] The reader may note that, unlike time domain simulation, the measured or predicted [26–29] FRF can be used directly without the requirement for a modal fit (which is also the case for the frequency domain stability solutions).

[1]Because the y-direction vibrations must be transformed into the time domain to determine the surface location error, the approach may be more properly referred to as a pseudo-frequency domain solution.

3. Fourier force model

If the cutting force model provided in Eq. (1) [10] that relates the tangential, F_t, and normal, F_n, cutting force components to the chip width (or axial depth of cut in peripheral end milling), b, and chip thickness, h, is applied, $F_y(\phi)$ can be expressed as shown in Eq. (2). In this equation, the summations account for all possible teeth within the cut, the circular tool path approximation has been applied, c is the chip load (or feed per tooth), and $g(\phi_i)$, is a switching function that is equal to 1 when tooth i is engaged in the cut and 0 otherwise. Also, the angle of each tooth (N total) at any instant in time is $\phi_i = \omega t + (2\pi/N)(i-1)$ for proportional teeth spacing, where ω is the spindle rotating frequency (in rad/s). See Fig. 2, where x is the tool feed direction.

$$\begin{aligned} F_t(\phi) &= k_t b h(\phi) + k_{te} b, \\ F_n(\phi) &= k_n b h(\phi) + k_{ne} b. \end{aligned} \tag{1}$$

$$F_y(\phi) = -b \begin{bmatrix} \frac{-k_t c}{2} \sum_{i=1}^{N} g(\phi_i)(1-\cos 2\phi_i) + \frac{k_n c}{2} \sum_{i=1}^{N} g(\phi_i) \sin 2\phi_i \\ -k_{te} \sum_{i=1}^{N} g(\phi_i) \sin \phi_i + k_{ne} \sum_{i=1}^{N} g(\phi_i) \cos \phi_i \end{bmatrix}. \tag{2}$$

The equivalent Fourier series for the y-direction cutting force, $F_y(\phi) = \sum_{i=1}^{N}(a_0 + \sum_{n=1}^{\infty}(a_n \cos n\phi_i + b_n \sin n\phi_i))$, can be written once the Fourier coefficients are determined. The a_0 term, for example, can be found using Eq. (3), where the integral for a full revolution of the selected tooth may be divided into three parts. These integrals are delineated by ϕ_1, which represents the cut entry angle in down milling or cut exit angle in up milling, and π, which defines the maximum angle that a tooth can be engaged in the cut (if ϕ is defined positive in a clockwise sense from the positive y axis). Considering a down milling cut, for example, only the middle of the three integrals in Eq. (3) is non-zero due to the switching function embedded in $F_y(\phi)$. Performing the relevant integration yields Eq. (4). For up milling, only the first integral in Eq. (3) is non-zero, but the procedure remains the same.

$$\begin{aligned} a_0 &= \frac{1}{2\pi} \int_0^{2\pi} F_y(\phi)\, d\phi \\ &= \frac{1}{2\pi} \left[\int_0^{\phi_1} F_y(\phi)\, d\phi + \int_{\phi_1}^{\pi} F_y(\phi)\, d\phi + \int_{\pi}^{2\pi} F_y(\phi)\, d\phi \right], \end{aligned} \tag{3}$$

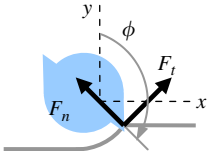

Fig. 2. Tangential and normal direction cutting forces for down milling.

$$a_0 = -\frac{bN}{2\pi} \times \left[-\frac{k_t c\phi}{2} + \frac{k_t c}{4}\sin 2\phi - \frac{k_n c}{4}\cos 2\phi + k_{te}\cos\phi + k_{ne}\sin\phi \right]_{\phi_1}^{\pi}. \quad (4)$$

The a_n coefficients are computed using Eq. (5) and the b_n coefficients using Eq. (6). Again, the integral can be partitioned using ϕ_1 and π as shown in Eq. (3). Closed-form equations for $n = 3, 4, 5,\ldots$ can be determined by observing the recursive patterns after integration. See Appendix A.

$$a_n = \frac{1}{\pi}\int_0^{2\pi} F_y(\phi)\cos n\phi \, d\phi, \quad (5)$$

$$b_n = \frac{1}{\pi}\int_0^{2\pi} F_y(\phi)\sin n\phi \, d\phi. \quad (6)$$

To accurately represent milling forces, however, it is also necessary to account for the influence of the teeth helix angle, β. This can be accomplished by separating the tool into A axial slices; each slice is assumed to have a zero helix angle and the slices are rotated relative to one another by the angle $\psi = 2\tan\beta db/d$, where db is the slice height and d is the cutter diameter (see Fig. 3). The Fourier series is now written as $F_y(\phi) = \sum_{j=1}^{A}\sum_{i=1}^{N}(a_0 + \sum_{n=1}^{\infty}(a_n\cos n\phi_i + b_n\sin n\phi_i))$, where $\phi_i = \omega t + (2\pi/N)(i-1) - \psi(j-1)$. The reader may note that the force record for non-proportionally spaced teeth may also be constructed by replacing $2\pi/N$ with the appropriate values.

As expected, the accuracy of the Fourier force signal depends on the number of coefficients included in the series. Fig. 4 shows a comparison of the y-direction force determined by time domain simulation and its Fourier series for $n = 5$ and 50. The cutting conditions are: up milling, 25% radial immersion (i.e., the radial depth of cut is equal to $0.25d$), $N = 4$, $\beta = 30^\circ$, $b = 1$ mm, $c = 0.1$ mm/tooth, $k_t = 700\,\mathrm{N/mm^2}$, $k_n = 210\,\mathrm{N/mm^2}$, $k_{te} = k_{ne} = 0$ N/mm, and $\omega = 300\pi$ rad/s (i.e., the spindle speed, Ω, is 9000 rev/min, or rpm).

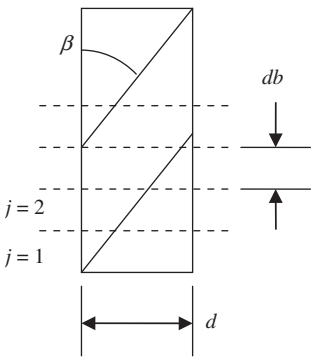

Fig. 3. Helix angle effects are incorporated using multiple axial slices of the cutter.

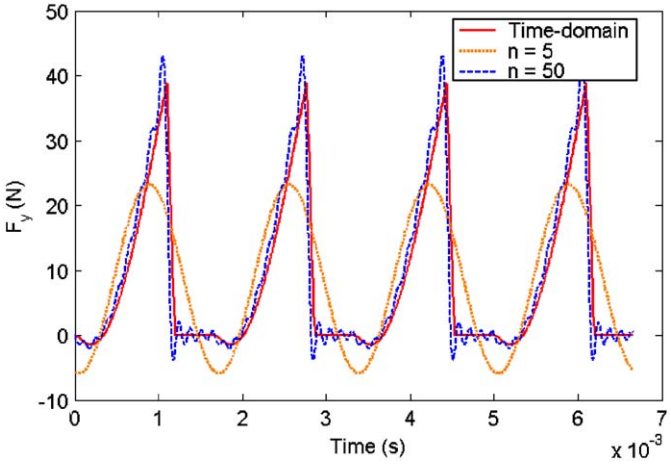

Fig. 4. Force reconstruction using time domain (solid line) and Fourier series (dotted line: $n = 5$; dashed line: $n = 50$). Additional coefficients increase force fidelity.

4. Harmonic balance approach

Section 2 provides an analytical solution for milling surface location prediction that relies on the system FRF in the direction normal to the tool feed direction and an appropriate force representation. However, the additional consideration of modal coupling between the x- and y-direction vibrations is possible with the development of a harmonic balance approach. As shown in Section 3, the cutting forces for periodic tool motion can be described as a trigonometric Fourier series expansion (Eq. (2) shows the y-direction result). In applying the harmonic balance approach, it is convenient to express the trigonometric Fourier series as a complex Fourier series. The first step in this process is to write the previously presented Fourier series coefficients as their complex series counterparts:

$$\vec{F}_o = \vec{a}_o,$$
$$\vec{F}_n = \tfrac{1}{2}(\vec{a}_n - \mathrm{i}\vec{b}_n), \quad n>0,$$
$$\vec{F}_n = \tfrac{1}{2}(\vec{a}_n + \mathrm{i}\vec{b}_n), \quad n<0, \quad (7)$$

where the vector forms for the forces and Fourier coefficients represent both the x- and y-directions. Here we note that the $\vec{F}_n$ expressions depend on the sign of the nth index, where corresponding positive and negative values of n give Fourier coefficients which are complex conjugates. Using these new coefficients, the complex representation of the cutting force vector becomes

$$\vec{F}(\phi) = [F_x(\phi) \quad 0 \quad \cdots \quad 0 \quad F_y(\phi) \quad 0 \quad \ldots \quad 0]^T = \sum_{m=1}^{N}\sum_{n=-\infty}^{\infty}\vec{F}_n e^{in(\omega t + 2\pi/N)}, \quad (8)$$

where ϕ is time dependent and the forces are assumed to be concentrated at the tool tip. We now seek a periodic solution for the tool motion (with respect to the tooth passing frequency) in the form of a complex Fourier series.

This is given by

$$\vec{X}_p(t) = \sum_{m=1}^{N} \sum_{n=-\infty}^{\infty} \vec{C}_{nm} e^{in\omega t}. \quad (9)$$

Substitution of Eqs. (8) and (9) into the governing equation of motion results in

$$\sum_{m=1}^{N} \sum_{n=-\infty}^{\infty} [-(n\omega)^2 M + in\omega C + K] \vec{C}_{nm} e^{in\omega t} = \sum_{m=1}^{N} \sum_{n=-\infty}^{\infty} \vec{F}_n e^{in(\omega t + (2\pi/N))}, \quad (10)$$

where M, C, and K are the spatial mass, damping, and stiffness matrices, respectively. The solution for each Fourier coefficient can be written for the mth cutting tooth as shown in Eq. (11).

$$\vec{C}_{nm} = H(n\omega) \vec{F}_n e^{in\phi_m}. \quad (11)$$

In this equation, the matrix expression $H(n\omega)$, which has the same dimensions as the modal matrices, is the tool FRF matrix

$$H(n\omega) = [-(n\omega)^2 M + in\omega C + K]^{-1}. \quad (12)$$

Since the tool tip is the only location with a non-zero cutting force, only a subset of the tool FRF matrix from Eq. (12), which contains the tool-tip direct and cross terms, is required to express the motions at the tool tip:

$$G(n\omega) = \begin{bmatrix} G_{xx}(n\omega) & G_{xy}(n\omega) \\ G_{yx}(n\omega) & G_{yy}(n\omega) \end{bmatrix}.$$

The final expression for the cutting tool periodic motion, under the assumption of chatter-free cutting, is given by Eq. (13). Similar to the frequency domain solution, surface location error is again determined by sampling the y-direction periodic motion vector at the appropriate time, i.e., cut entry for up milling or cut exit for down milling:

$$\vec{X}_p(t) = \sum_{m=1}^{N} \sum_{n=-\infty}^{\infty} G(n\omega) \vec{F}_n e^{in(\omega t + (2\pi/N))}. \quad (13)$$

5. Numerical demonstrations

To numerically verify the two approaches, comparisons between a comprehensive time domain simulation [12], which incorporates the effects of the true cycloidal tool path and helix angle, and the analytical solutions have been completed. Fig. 5 shows the results for 50% radial immersion up milling cuts carried out at spindle speeds from 6900 to 7700 rpm ($N = 4$, $\beta = 30^\circ$, $d = 12.7$ mm diameter, $c = 0.1$ mm/tooth, $b = 1$ and 2.5 mm, $k_t = 700\,\mathrm{N/mm^2}$, $k_n = 210\,\mathrm{N/mm^2}$, $k_{te} = k_{ne} = 0\,\mathrm{N/mm}$, symmetric structural dynamics with a stiffness of 1×10^7 N/m, 1% viscous damping, and 500 Hz natural frequency, f_n). Reasonable agreement is seen between the surface location error predicted by time domain (open circles), frequency domain (solid line), and harmonic balance (dotted line). To interpret the figure, a positive error indicates an overcut surface for up milling (the opposite is true for down milling). A source of disagreement between the time domain and analytical results is that the analytical solutions do not consider the variation in radial immersion due to tool deflections, which is inherently included in the time domain simulation.

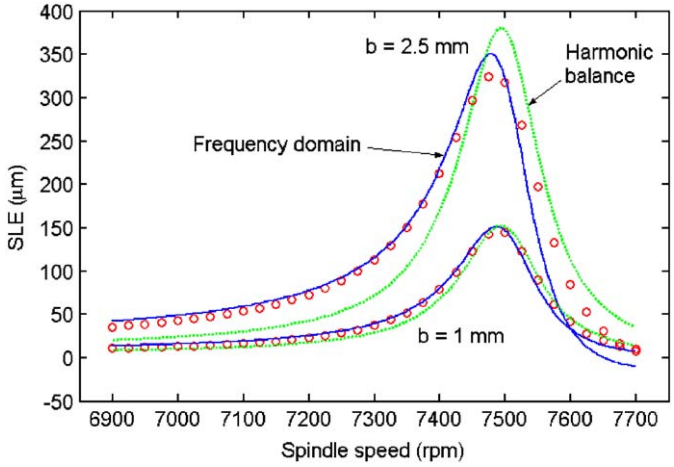

Fig. 5. Comparison between time domain (open circles), frequency domain (solid line), and harmonic balance (dotted line) surface location error, SLE, simulations. Results for two axial depths of cut, 1 and 2.5 mm, are provided.

Next, analytical simulations were completed for the same system over a range of axial depths and spindle speeds to determine the variation in surface location error within a single stable region. The surface location error contours predicted by the frequency domain and harmonic balance solutions (now represented as a height map for the control variables b and spindle speed), as well as the corresponding stability lobe diagram [23] are provided in Fig. 6. It is observed that at the traditional 'best' spindle speed, $\Omega = 60 f_n/Nk = 7500$ rpm ($k = 1$) near the lobe peak, the surface location error is highly sensitive to variations in spindle speed (for fixed dynamics) or the system natural frequency (for a fixed spindle speed).

Simulations were also carried out for a two degree-of-freedom response (the x- and y-direction dynamics were set equal) under 50% radial immersion down milling with $N = 4$, $\beta = 12^\circ$, $d = 12.7$ mm diameter, $c = 0.1$ mm/tooth, $b = 2$ mm, $k_t = 700\,\mathrm{N/mm^2}$, $k_n = 210\,\mathrm{N/mm^2}$, and $k_{te} = k_{ne} = 2\,\mathrm{N/mm}$. The stability lobe diagram, surface location error variation with spindle speed, and dynamic response are provided in Fig. 7. In this case, it is seen that the error is worse to the left of the stable region due to the combination of the overlapping stability boundaries.

Finally, the well-known variation of surface location error along the tool axis (z-direction) for helical cutting edges was computed (see, e.g., Fig. 9.50 in Ref. [30]). Fig. 8 shows the results for 50% radial immersion up milling with the same

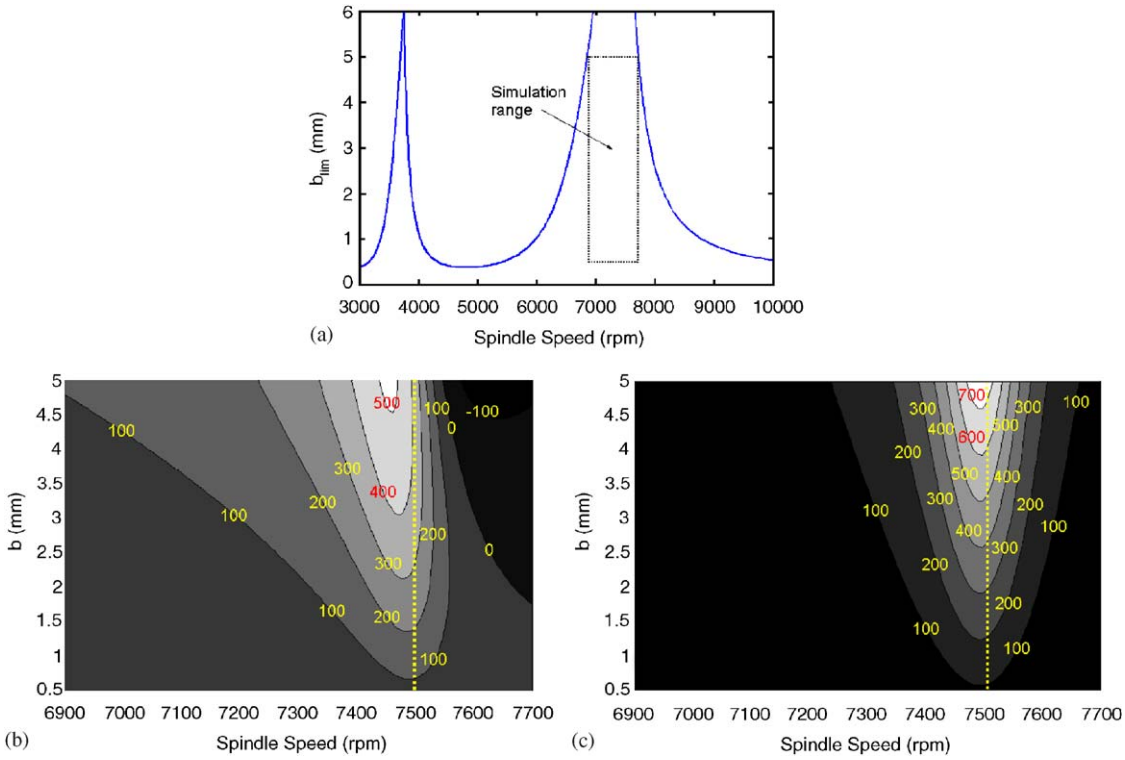

Fig. 6. Surface location error variation for 50% radial immersion up milling over a range of axial depths and spindle speeds for single degree-of-freedom system dynamics: (a) stability lobe diagram with simulation range; (b) frequency domain surface location error contours (error values given in μm); and (c) harmonic balance results. It is seen that the error varies substantially near the traditionally-selected 'best' spindle speed at 7500 rpm.

specifications provided for Fig. 5 at $\Omega = 7500$ rpm and $b = 5$ mm. The strong variation of surface location error shown in Fig. 8 occurs because points along the cutting edge (in the z-direction) from the bottom of the cutter to the full axial depth produce the surface at progressively later points in time as the cutter vibration state varies continuously. This is handled in the analytical approaches by changing the times at which the $y(t)$ vector is sampled to determine surface location error. For axial locations not at the tool point, the time vector is sampled later than the cut entry (up milling) or exit (down milling) by $\psi(j-1)/\omega$, where $j = 1$ represents the axial slice at the tool point.

It is interesting to note that in all the numerical demonstrations the surface location error predicted by the analytical approaches did not show a strong dependence on the number of Fourier terms included in the force representation. Because surface location error is dominated by the force content near the system resonance(s), particularly for the lowly damped dynamic systems typically encountered in milling, it is not necessary to accurately represent the cutting force in the time domain. Rather, only a few Fourier terms are sufficient provided the fundamental tooth passing frequency or harmonic(s) located near the system natural frequency(s) are accurately represented. While the actual cutting signal may contain many harmonics far from the system resonance(s), the relative contribution of the displacement induced by these spectral peaks is small.

6. Experimental results

To obtain experimental verification of the analytical surface location error solutions, cutting tests were completed on a single degree-of-freedom flexure in order to provide a simple dynamic system. The flexure and tool were selected so that the flexure response (in the flexible direction) was much less stiff than either the tool point response or the flexure response in the orthogonal direction. Fig. 9 shows the measured frequency response functions (obtained by impact testing) and coordinate directions for the flexure.

The y-direction frequency response shown in Fig. 9 was used to construct stability lobes for 100% radial immersion cuts with $c = 0.15$ mm/tooth and $N = 2$ in the x-direction. Cutting coefficients for the 6061-T651 aluminum workpiece were determined to be $k_t = 700\,\mathrm{N/mm^2}$, $k_n = 210\,\mathrm{N/mm^2}$, and $k_{te} = k_{ne} = 2\,\mathrm{N/mm}$ from independent cutting tests [10]. Experimental validation of the stability lobe diagram is provided in Fig. 10.

Next, surface location error tests were completed by first preparing workpieces with 5.4 mm wide by 10 mm tall ribs that were then finish machined on each face to reduce the rib width for the top 5 mm (the bottom 5 mm was left untouched to provide a control for the experiments). The x-direction down milling cutting conditions for the finishing passes on each side of the ribs were 1 mm radial depth of cut (4% radial immersion for the 25.4 mm

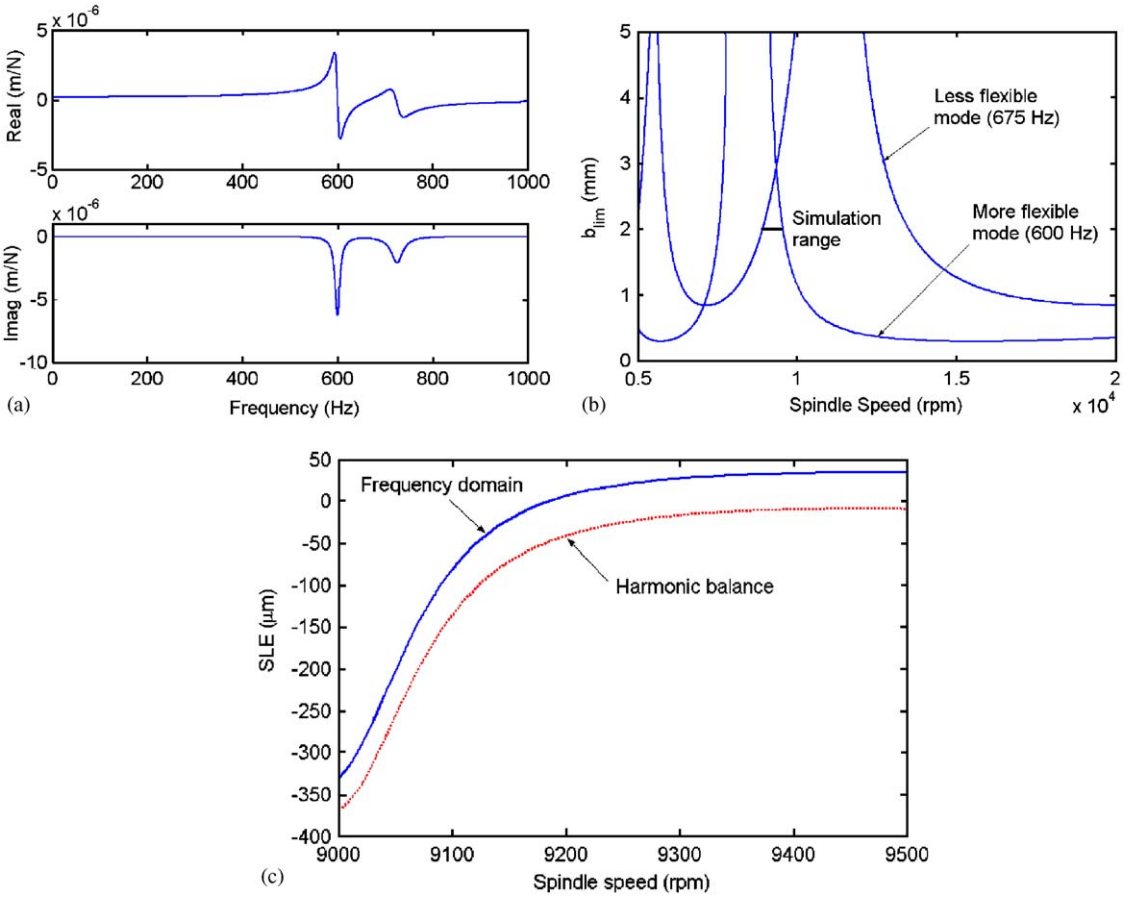

Fig. 7. Surface location error for two degree-of-freedom system dynamics: (a) frequency response function for both x- and y-directions (mode 1: 8×10^6 N/m stiffness, 1% damping, $f_n = 600$ Hz; mode 2: 12×10^6 N/m stiffness, 2% damping, $f_n = 675$ Hz); (b) stability lobe diagram with simulation range identified; and (c) surface location error results. The combined effect of the two modes leads to higher error to the left of the stable region, rather than the right as seen in Figs. 5 and 6.

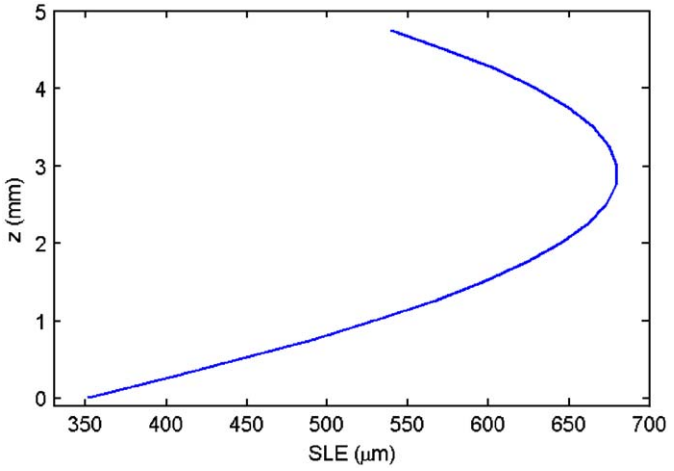

Fig. 8. Variation in surface location error with axial depth due to helix angle at 7500 rpm (frequency domain result shown). The free end of the tool (i.e., the tool point) corresponds to the $z = 0$ value.

diameter tool), $b = 5$ mm, and $c = 0.1$ mm/tooth. The cutting geometry is shown in Fig. 11.

Six ribs were machined at spindle speeds ranging from 13 425 to 13 675 rpm in increments of 50 rpm. This approximately centered the tests on the 'best' spindle speed for the flexure-workpiece natural frequency of 451.7 Hz (5.35×10^6 N/m stiffness and 0.35% damping). After machining, the rib widths were measured at three locations along the rib height using a touch-probe coordinate measuring machine (2 mm diameter ruby probe). At each height, A, B, and C (see Fig. 12), 23 points were recorded on each side of the ribs and the rib width was determined from straight-line fits to these points. These points were obtained at 2 mm increments and the total measurement range was located near the center of the ribs (25 mm from each end) to avoid transient contributions to the rib width. The measurements at point A were used to verify that each rib started with the same width, while the measurements at B and C served to demonstrate the dependence of surface location error on the axial location along the helical cutting edge.

The experimental surface location error results and frequency domain approach predictions are shown in Fig. 13. Additionally, the two standard deviation error bars for the coordinate measuring machine rib width measurements are provided (12 total measurements were completed for each rib). These are included to show that

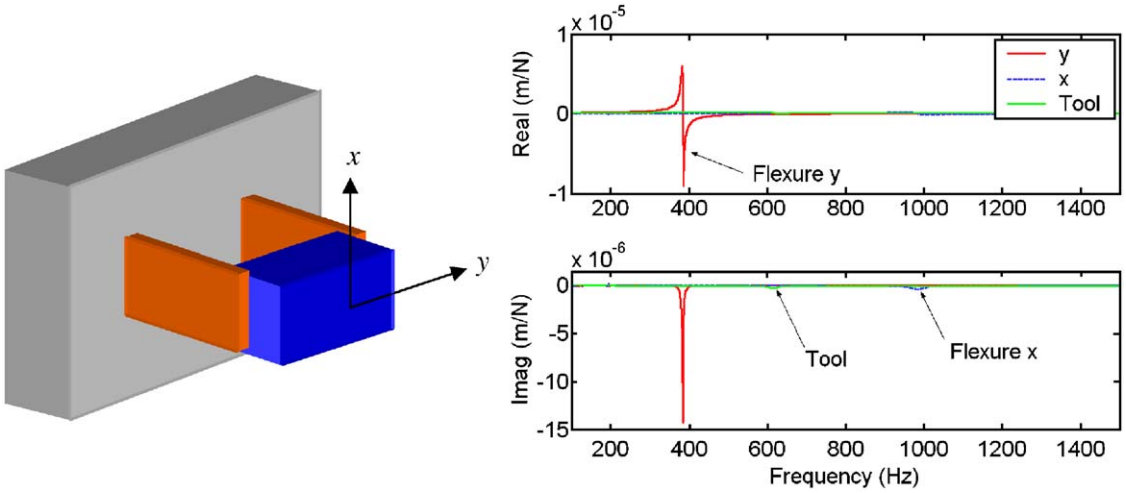

Fig. 9. Frequency response functions for flexure in x- and y-directions and cutting tool (symmetric response). The flexure was 40 times more flexible in the y-direction.

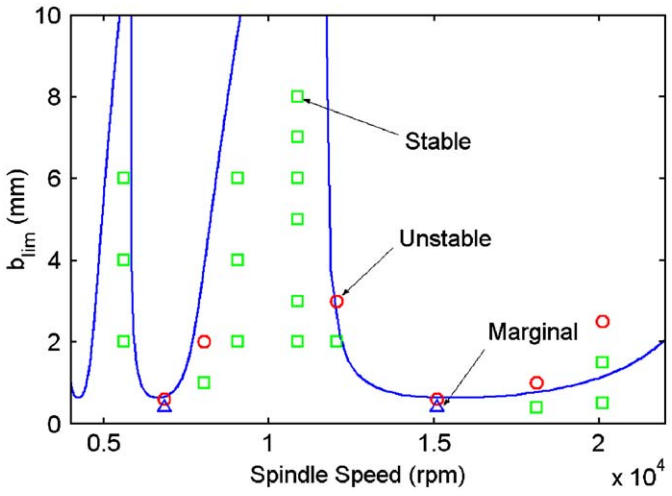

Fig. 10. Stability lobe verification for flexure setup. Slotting cuts in the y-direction were performed and chatter determined from the surface finish and audio signal.

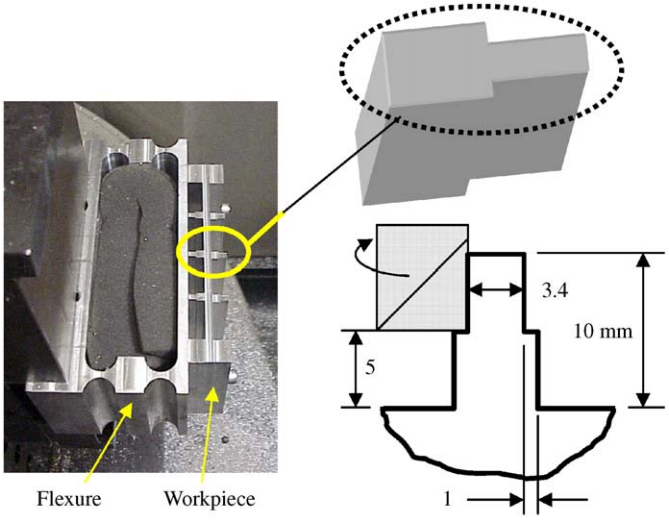

Fig. 11. Geometry and setup for surface location error down milling tests. The ribs were prepared first, then finish machined in a single setup. The foam inside the flexure was used to increase the damping.

the measurement repeatability[2] was a small fraction of the overall surface location variation (1–2 μm). The trend of undercut to overcut as the tooth passing frequency passes through the flexure natural frequency is seen with a total experimental variation of approximately 250 μm for a 200 rpm spindle speed change. The agreement with analytical results is reasonable, including the trend of increasing difference between the B and C surface location error values near resonance.

7. Conclusions

This paper provided numerical and experimental validation of two new analytical solutions for the problem of surface location error in milling. First, a frequency domain approach was presented which considers the deflections normal to the desired surface and the corresponding frequency response function. The primary benefits of this

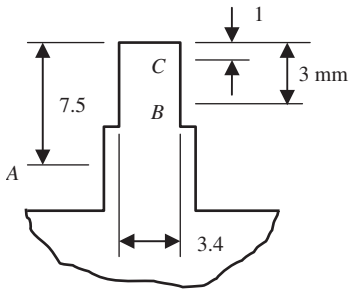

Fig. 12. Coordinate measuring machine measurement locations A, B, and C.

[2]The measurement repeatability does not provide an indication of the coordinate measuring machine accuracy. We estimate a measurement uncertainty of <5 μm for the work volume required for the parts in this study.

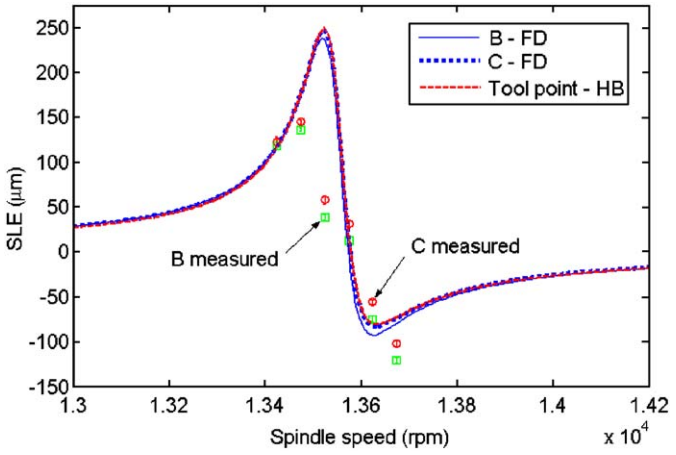

Fig. 13. Comparison of experimental and analytical surface location error results. Data points were recorded using a coordinate measuring machine at locations B and C along the rib height. The frequency domain (FD) predictions were made for the same axial locations along the tool (dotted line: B; solid line: C). The harmonic balance (HB) prediction for the tool point is also provided for comparison.

approach are: (1) the ability to use the measured or predicted frequency response function directly; and (2) its compatibility with frequency domain stability solutions available in the literature. Second, a harmonic balance solution was provided which enables the consideration of modal coupling between the feed and surface normal dynamics, as well as prediction of the steady-state deflections in these two directions.

Acknowledgements

The authors gratefully acknowledge partial financial support from the National Science Foundation (DMI-0238019 and CMS-0348288), Office of Naval Research (2003 Young Investigator Program), and BWXT Y-12.

Appendix A. Fourier force coefficients

The Fourier y-direction force coefficients, a_n and b_n, determined from Eqs. (5) and (6) are provided here.

$$a_1 = -\frac{bN}{\pi}\left[\begin{array}{l} k_t c\left(-\frac{1}{4}\sin\phi + \frac{1}{12}\sin 3\phi\right) + k_n c\left(-\frac{1}{4}\cos\phi - \frac{1}{12}\cos 3\phi\right) \\ \quad + k_{te}\left(\frac{1}{4}\cos 2\phi\right) + k_{ne}\left(\frac{1}{2}\phi + \frac{1}{4}\sin 2\phi\right) \end{array}\right]_{\phi_1}^{\pi}, \tag{A.1}$$

$$a_2 = -\frac{bN}{\pi}\left[\begin{array}{l} k_t c\left(\frac{1}{4}\phi - \frac{1}{4}\sin 2\phi + \frac{1}{16}\sin 4\phi\right) + k_n c\left(-\frac{1}{16}\cos 4\phi\right) \\ \quad + k_{te}\left(-\frac{1}{2}\cos\phi + \frac{1}{6}\cos 3\phi\right) + k_{ne}\left(\frac{1}{2}\sin\phi + \frac{1}{6}\sin 3\phi\right) \end{array}\right]_{\phi_1}^{\pi}, \tag{A.2}$$

$$a_n = -\frac{bN}{\pi}\left[\begin{array}{l} k_t c\left(-\frac{1}{2n}\sin n\phi + \frac{1}{4(n-2)}\sin(n-2)\phi + \frac{1}{4(n+2)}\sin(n+2)\phi\right) \\ \quad + k_n c\left(\frac{1}{4(n-2)}\cos(n-2)\phi - \frac{1}{4(n+2)}\cos(n+2)\phi\right) \\ \quad + k_{te}\left(-\frac{1}{2(n-1)}\cos(n-1)\phi + \frac{1}{2(n+1)}\cos(n+1)\phi\right) \\ \quad + k_{ne}\left(\frac{1}{2(n-1)}\sin(n-1)\phi + \frac{1}{2(n+1)}\sin(n+1)\phi\right) \end{array}\right]_{\phi_1}^{\pi}, \quad n = 3, 4\ldots, \tag{A.3}$$

$$b_1 = -\frac{bN}{\pi}\left[\begin{array}{l} k_t c\left(\frac{3}{4}\cos\phi - \frac{1}{12}\cos 3\phi\right) + k_n c\left(\frac{1}{4}\sin\phi - \frac{1}{12}\sin 3\phi\right) \\ \quad + k_{te}\left(-\frac{1}{2}\phi + \frac{1}{4}\sin 2\phi\right) + k_{ne}\left(-\frac{1}{4}\cos 2\phi\right) \end{array}\right]_{\phi_1}^{\pi}, \tag{A.4}$$

$$b_2 = -\frac{bN}{\pi}\left[\begin{array}{l} k_t c\left(\frac{1}{4}\cos 2\phi - \frac{1}{16}\cos 4\phi\right) + k_n c\left(\frac{1}{4}\phi - \frac{1}{16}\sin 4\phi\right) \\ \quad + k_{te}\left(-\frac{1}{2}\sin\phi + \frac{1}{6}\sin 3\phi\right) + k_{ne}\left(-\frac{1}{2}\cos\phi - \frac{1}{6}\cos 3\phi\right) \end{array}\right]_{\phi_1}^{\pi}, \tag{A.5}$$

$$b_n = -\frac{bN}{\pi}\left[\begin{array}{l} k_t c\left(\frac{1}{2n}\cos n\phi - \frac{1}{4(n-2)}\cos(n-2)\phi - \frac{1}{4(n+2)}\cos(n+2)\phi\right) \\ \quad + k_n c\left(\frac{1}{4(n-2)}\sin(n-2)\phi - \frac{1}{4(n+2)}\sin(n+2)\phi\right) \\ \quad + k_{te} c\left(-\frac{1}{2(n-1)}\sin(n-1)\phi + \frac{1}{2(n+1)}\sin(n+1)\phi\right) \\ \quad + k_{ne} c\left(-\frac{1}{2(n-1)}\cos(n-1)\phi - \frac{1}{2(n+1)}\cos(n+1)\phi\right) \end{array}\right]_{\phi_1}^{\pi}, \quad n = 3, 4, \ldots. \tag{A.6}$$

References

[1] W. Kline, R. DeVor, I. Shareef, The prediction of surface accuracy in end milling, Journal of Engineering for Industry 104 (1982) 272–278.

[2] W. Kline, R. DeVor, J. Lindberg, The prediction of cutting forces in end milling with application to cornering cuts, International Journal of Machine Tool Design Research 22 (1982) 7–22.

[3] J. Tlusty, Effect of end milling deflections on accuracy, in: R.I. King (Ed.), Handbook of High Speed Machining Technology, Chapman & Hall, New York, 1985, pp. 140–153.

[4] J. Sutherland, R. DeVor, An improved method for cutting force and surface error prediction in flexible end milling systems, Journal of Engineering for Industry 108 (1986) 269–279.

[5] D. Montgomery, Y. Altintas, Mechanism of cutting force and surface generation in dynamic milling, Journal of Engineering for Industry 113 (2) (1991) 160–168.

[6] S. Smith, J. Tlusty, An overview of modeling and simulation of the milling Process, Journal of Engineering for Industry 113 (2) (1991) 169–175.

[7] Y. Altintas, D. Montgomery, E. Budak, Dynamic peripheral milling of flexible structures, Journal of Engineering for Industry 114 (2) (1992) 137–145.

[8] Y. Tarng, C. Liao, H. Li, A mechanistic model for prediction of the dynamics of cutting forces in helical end milling, International Journal of Modeling and Simulation 14 (2) (1994) 92–97.

[9] T.L. Schmitz, J. Ziegert, Examination of surface location error due to phasing of cutter vibrations, Precision Engineering 23 (1) (1999) 51–62.

[10] Y. Altintas, Manufacturing Automation, Cambridge University Press, Cambridge, UK, 2000.

[11] B.P. Mann, P.V. Bayly, M.A. Davies, J.E. Halley, Limit cycles, bifurcations, and accuracy of the milling process, Journal of Sound and Vibration 277 (2004) 31–48.

[12] T.L. Schmitz, J. Couey, E. Marsh, M. Tummond, The role of cutter eccentricity on surface finish and milling forces, in: Proceedings of ASME International Mechanical Engineering Congress and Exposition Anaheim, CA, 2004, IMECE2004-60232.

[13] W.-S. Yun, J. Ko, D.-W. Cho, K. Ehmann, Development of a virtual machining system, Part 2: prediction and analysis of a machined surface error, International Journal of Machine Tools and Manufacture 42 (2002) 1607–1615.

[14] B. P. Mann, N. K. Garg, K. A. Young, A. M. Helvey, Milling bifurcations from structural asymmetry and nonlinear regeneration, Nonlinear Dynamics, in press.

[15] R.N. Arnold, The mechanism of tool vibration in the cutting of steel, Proceedings of the Institution of Mechanical Engineers 154 (4) (1946) 261–284.

[16] S.A. Tobias, Machine-Tool Vibration, Blackie and Sons Ltd., Glasgow, Scotland, 1965.

[17] S.A. Tobias, W. Fishwick, The chatter of lathe tools under orthogonal cutting conditions, Transactions of the ASME 80 (1958) 1079.

[18] S.A. Tobias, W. Fishwick, Theory of regenerative machine tool chatter, The Engineer 205 (1958).

[19] J. Tlusty, M. Polocek, The stability of the machine-tool against self-excited vibration in machining, in: Proceedings of the International Research in Production Engineering Conference Pittsburgh, PA, 1963, p. 465.

[20] F. Koenisberger, J. Tlusty, Machine Tool Structures, vol. I: Stability Against Chatter, Pergamon Press, Oxford, 1967.

[21] H. Merrit, Theory of self-excited machine tool chatter, Journal of Engineering for Industry 87 (4) (1965) 447–454.

[22] J. Tlusty, W. Zaton, F. Ismail, Stability lobes in milling, Annals of the CIRP 32 (1) (1983) 309–313.

[23] Y. Altintas, E. Budak, Analytical prediction of stability lobes in milling, Annals of the CIRP 44 (1) (1995) 357–362.

[24] E. Budak, Y. Altintas, Analytical prediction of chatter stability conditions for multi-degree of freedom systems in milling. Part I: Modeling, Part II: applications, Journal of Dynamic Systems, Measurement and Control, Transactions of the ASME 120 (1998) 22–36.

[25] T. Insperger, B.P. Mann, G. Stépán, P.V. Bayly, Stability of up-milling and down-milling, Part 1: alternative analytical methods, International Journal of Machine Tools and Manufacture 43 (2003) 25–34.

[26] T.L. Schmitz, G.S. Duncan, Three-component receptance coupling substructure analysis for tool point dynamics prediction, Journal of Manufacturing Science and Engineering, 2005, to appear.

[27] G.S. Duncan, M. Tummond, T.L. Schmitz, An investigation of the dynamic absorber effect in high-speed machining, International Journal of Machine Tools and Manufacture 45 (2005) 497–507.

[28] T.L. Schmitz, M. Davies, M. Kennedy, Tool point frequency response prediction for high-speed machining by RCSA, Journal of Manufacturing Science and Engineering 123 (2001) 700–707.

[29] T.L. Schmitz, Predicting high-speed machining dynamics by substructure analysis, Annals of the CIRP 49 (1) (2000) 303–308.

[30] J. Tlusty, Manufacturing Processes and Equipment, Prentice-Hall, Upper Saddle River, NJ, 1999.